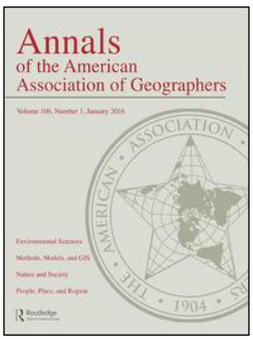

Annals of the American Association of Geographers

ISSN: 2469-4452 (Print) 2469-4460 (Online) Journal homepage: http://www.tandfonline.com/loi/raag21

Cellular Automata Modeling of Land-Use/Land-Cover Dynamics: Questioning the Reliability of Data Sources and Classification Methods

Yulia Grinblat, Michael Gilichinsky & Itzhak Benenson

To cite this article: Yulia Grinblat, Michael Gilichinsky & Itzhak Benenson (2016) Cellular Automata Modeling of Land-Use/Land-Cover Dynamics: Questioning the Reliability of Data Sources and Classification Methods, Annals of the American Association of Geographers, 106:6, 1299-1320, DOI: 10.1080/24694452.2016.1213154

To link to this article: http://dx.doi.org/10.1080/24694452.2016.1213154

Cellular Automata Modeling of Land-Use/Land-Cover Dynamics: Questioning the Reliability of Data Sources and Classification Methods

Yulia Grinblat,* Michael Gilichinsky,† and Itzhak Benenson‡

*Department of Geography and Human Environment and The Porter School of Environmental Studies, Tel Aviv University
†Research and Development Center, Ariel University
‡Department of Geography and Human Environment, Tel Aviv University

Based on four time intervals within a forty-year period of observation, we construct land-use/land-cover (LULC) maps and estimate the transition probabilities between six LULC states. The maps and transition probability matrices (TPMs) were built based on the high-resolution aerial photos and 30-m multispectral Landsat images for the same years. We considered the TPM constructed from manual classification of the aerial photos as a reference and compared it to the TPM constructed from the Landsat image classified with several methods: mean-shift segmentation followed by random forest classification and three pixel-based methods popular in cellular automata (CA) studies: *K*-means, iterative self-organizing data analysis techniques (ISODATA), and maximum likelihood. For each classification method, the TPMs were constructed and compared to the TPMs for the aerial photos. We prove that the goodness-of-fit of maps obtained with the three pixel-based methods was insufficient for estimating the LULC TPM. The LULC maps obtained with the object-based classification fit well to those based on the aerial photos, but the estimates of TPM were yet qualitatively different. This article raises doubts regarding the adequacy of Landsat data and standard classification methods for establishing LULC CA model rules and calls for the careful reexamination of the entire land-use CA framework. We appeal for a new view of the CA modeling methodology: It should be based on a long-term series of carefully validated LULC maps that portray different types of land-use dynamics and land planning systems over long and representative periods of population and economic growth. *Key Words: cellular automata, Landsat images, land-use/land-cover changes, Markov transition probabilities matrices, validation of remote sensing classification methods.*

我们根据在四十年观察期间的四次间隔, 建构土地使用/地表覆盖 (LULC) 的地图, 并评估六个 LULC 州的转移可能性。这些地图与转移概率矩阵 (TPMs), 是根据同年的高分辨率航摄照片和三十公尺的多光谱地球卫星影像建构之。我们考量从航摄照片的人工分类所建立的TPM作为参照, 并将其与以若干方法进行分类的地球卫星影像所建构的TPM进行比较：均质平移分割, 以及随后的随机森林分类, 还有细胞自动机 (CA) 研究中以像素为基础的的三大流行方法：K-平均数, 迭代自组织数据分析演算法 (ISODATA), 以及最大化可能性。我们对每个分类方法建立 TPMs 并与航摄照片的TPMs进行比较。我们証实, 透过三个以像素为基础的方法所取得的地图适合度, 对评估 LULC TPM 而言并不充足。以物件为基础的分类法所获得的LULC地图, 相当符合根据航摄照片的地图, 但TPM的估计在数值上却仍不同。本文提出有关地球卫星影像和标准分类方法在建立 LULC CA 模型规则上的适切性之质疑, 并呼吁再次对整个土地使用 CA 架构进行细緻的检验。我们恳求对 CA 模式化方法的崭新观点：它应该根据描绘在人口及经济成长的长期代表週期中, 不同种类的土地使用动态和土地使用规划系统、且经过长时间仔细验证的 LULC 地图。*关键词： 细胞自动机, 地球卫星图像, 土地使用／地表覆盖变迁, 马尔科夫转移概率矩阵, 遥感分类方法的验证。*

Con base en intervalos temporales de cuatro dentro de un período de observación de cuarenta años, construimos mapas de uso del suelo/cobertura de la tierra (LULC) y calculamos las probabilidades de transición entre seis LULC estatales. Los mapas y las matrices de probabilidades de transición (TPMs) fueron construidos con base en aerofotos de alta resolución e imágenes Landsat multiespectrales de 30-m para los mismos años. Tomamos como referencia la TPM construida a partir de la clasificación manual de las aerofotos y la comparamos con la TPM construida de la imagen Landsat clasificada con varios métodos: segmentación de cambio mediano seguida por clasificación forestal aleatoria, y tres métodos basados en pixeles que son populares en los estudios de modelos celulares autómatas (CA): el *K-means*, las técnicas de análisis de datos iterativos auto-organizados (ISODATA) y la probabilidad máxima. Para cada método de clasificación, las TPMs fueron construidas y comparadas con las TPMs para las aerofotos. Probamos que la bondad de ajuste de los mapas obtenidos con los tres

Annals of the American Association of Geographers, 106(6) 2016, pp. 1299–1320 © 2016 by American Association of Geographers
Initial submission, May 2015; revised submissions, February and June 2016; final acceptance, June 2016
Published by Taylor & Francis, LLC.

métodos basados en pixeles era insuficiente para calcular la TPM de LULC. Los mapas de LULC obtenidos con la clasificación basada en objeto encajaron bien con los basados en aerofotos, aunque los cálculos de la TPM eran todavía cualitativamente diferentes. Este artículo levanta dudas sobre la idoneidad de los datos Landsat y los métodos de clasificación corrientes para establecer reglas del modelo CA LULC y clama por un cuidadoso reexamen de todo el marco CA de uso del suelo. Somos partidarios de una nueva visión de la metodología modeladora de los CA: Esta debe basarse en una serie a largo plazo de mapas LULC cuidadosamente validados que representen los diferentes tipos de dinámica de uso del suelo y sistemas de planificación de la tierra sobre largos y representativos períodos de crecimiento de la población y la economía. *Palabras clave: celulares autómatas, imágenes Landsat, cambios de uso del suelo/cobertura del suelo, matrices Markov de probabilidades de transición, validación de métodos de clasificación por percepción remota.*

Conceptual simplicity and the ability of explicit representation of landscapes and their changes make cellular automata (CA) a standard tool for simulating urban and regional land-use dynamics (White and Engelen 1993; Clarke, Hoppen, and Gaydos 1996; Balmann 1997; Stevens, Dragicevic, and Rothley 2007). CA provide a convenient and flexible framework and serve as a background for the implementation of various approaches to the land-use/land-cover (LULC) dynamics modeling, including fuzzy set theory (Wu 1998), innovation diffusion (Clarke, Hoppen, and Gaydos 1996; Candau and Clarke 2000), development theory (Batty, Xie, and Sun 1999), multicriteria evaluation (Wu and Webster 1998), case-based reasoning (Du et al. 2010), artificial neural networks (Li and Yeh 2001; Pijanowski et al. 2002), logistic regression (Verburg et al. 2002; Wu 2002), and others. The potential of CA for modeling LULC dynamics has been widely recognized (Maria de Almeida et al. 2003; Kamusoko et al. 2009; Guan et al. 2011; Mitsova, Shuster, and Wang 2011).

The major source of data for CA modeling is remote sensing (RS) multispectral imagery that is classified for establishing land uses and covers. Typically, the adequacy of LULC classification is validated based on the comparison between the classified image and either the reference map or a sample of ground control points (GCPs). Typical overall goodness of fit is 80 to 90 percent (see Table 1). The rules of CA regard LULC changes that are the derivatives of the LULC maps, however. Misclassification could have a disproportional effect on the estimates of these changes (Hall et al. 1991). This is especially relevant for the changes that occur during a typical CA LULC modeling time interval of five to fifteen years: The lands for which use has changed during such a time interval comprise, at most, a few percent of the areas investigated.

The typical size of an investigated area varies between several hundred and several thousand square kilometers and the changes are mostly spread over the borders of relatively homogeneous land-use patches representing long-standing built-up areas, roads, agricultural and open areas, forests, and water surfaces. In these circumstances, the likely classification of the entire study area does not guarantee an adequate view of the area's *changes*—the total amount and location—which are critical for establishing the rules of the CA model.

Strangely enough, the adequacy of the output of RS classification methods is far from the focus of CA research. Despite several important studies that demonstrate the importance of classification-dependent issues for CA modeling, the majority of modeling studies take the outputs of the imagery classification for granted and focus on model calibration (Li and Yeh 2001; Logofet and Korotkov 2002; Silva and Clarke 2002; Straatman, White, and Engelen 2004; Pijanowski et al. 2005; Dietzel and Clarke 2007; Torrens 2011). Indeed, CA dynamics are highly sensitive to the model settings, including spatial and temporal resolution, and the rules' parameters (Pontius 2002; Chen and Mynett 2003; Liu and Andersson 2004; Pontius and Malizia 2004; Jantz and Goetz 2005; Dietzel and Clarke 2006; Wang, Zheng, and Zang 2012; Blanchard, Pontius, and Urban 2015). Model setting and parameters are defined by the classified maps of the LULC changes; erroneous classification will result in inadequate setting and transition rules regardless of the methods of the rules' calibration and parameter estimation.

Generally, urban CA models are calibrated by tailoring the parameters that control transition rules (Torrens 2011). The Dutch Environment Explorer (Hagen-Zanker et al. 2005) provides a comprehensive example of calibration and validation that is performed at two levels—regional and local. The dynamics at the local level are defined by the CA model, and its parameters are calibrated based on historical data using fuzzy-kappa statistics. At the next stage, the likelihood of the LULC maps generated by the proposed set of rules is judged by the experts. Validation also involves comparison of the

Table 1. The remote sensing data and classification methods employed in the cellular automata models of land-use/land-cover changes

No.	Publication	Data source	Classification method	Cell size (m)	The number and list of the LULC classes	Validation versus	k	P_C (%)	Study area
1	Mitsova, Shuster, and Wang (2011)	National Land Cover data set	Generalization	30	5: water, woodland, cropland, wetland, urban	NR	NR	NR	Cincinnati–Middletown, USA
2	Shafizadeh, Moghadam, and Helbich (2013)	Landsat (MSS, TM, ETM+)	ML	30	5: built-up, water, wetlands, forest and green space, open land and cropland	250 GCPs	0.84–0.86	71–83%	India
3	Mondal and Southworth (2010)	Landsat (MSS, TM), Aster	Hybrid (ISODATA, ML)	30	3: forest, bare soil, water	143 GCPs	0.89	94%	India
4	Kamusoko et al. (2009)	Landsat (MSS, TM, ETM+), Aster	Hybrid (ISODATA, ML)	30, 15	5: agriculture, woodland, mixed rangeland, bare land, water	600 GCPs	0.83–0.88	86–90%	Zimbabwe
5	Puertas, Henríquez, and Meza (2014)	Landsat (MSS, TM, ETM+)	Support vector machine	30	4: vegetation, agriculture, bare soil, urban	908 GCPs	0.64–0.78	65–71%	Santiago, Chile
6	Vaz et al. (2012)	CORINE Land Cover data set	Generalization	100	5: urban, agriculture, forest, wetland, water	NR	NR	NR	Portugal
7	Fan, Wang, and Wang (2008)	Landsat (TM, ETM+)	ML	30	9: urban, forest, development, farmland, orchard, paddy-field, grass-field, water, dike-pond land	690 GCPs	0.82–0.88	86.5–91.6%	Pearl River Delta, China
8	Arsanjani, Kainz, and Mousivand (2011)	Landsat (TM, ETM+)	Visual interpretation	30	5: built-up, agricultural lands, public parks, open lands, water	NR	0.88–0.91	NR	Tehran, Iran
9	Myint and Wang (2006)	Landsat (MSS, TM, ETM+)	ML	30	7: water, agriculture, woodland, grass, residential, commercial, shrubs	225 GCPs	0.83–0.87	85.8–89.3%	Norman, Oklahoma, USA
10	Araya and Cabral (2010)	Landsat (TM), SPOT, LISS-III	Multiresolution segmentation	30	7: built-up area, urban vegetation, irrigated land, nonirrigated, forest cover, bare land, water	240 GCPs	0.83–0.86	87.7–92.5%	Lisbon, Portugal

(*continued on next page*)

Table 1. The remote sensing data and classification methods employed in the cellular automata models of land-use/land-cover changes *(Continued)*

No.	Publication	Data source	Classification method	Cell size (m)	The number and list of the LULC classes	Validation versus	k	P_C (%)	Study area
11	Xi et al. (2010)	Landsat (TM)	Not mentioned	60	7: urban, agricultural, forest, water, rural, mine, barren	NR	0.81–0.85	85.5–88.5%	Shenyang-Fushun, China
12	Norman, Feller, and Villareal (2012)	Landsat (MSS, TM)	Classification and regression tree algorithm	30	10: open water, urban, barren land, deciduous forest, evergreen forest, shrub, cultivated crops and pasture, wetlands, recreational grasses	700 GCPs	0.80–0.85	>80%	Santa Cruz Watershed, Arizona, USA, and Sonora, Mexico
13	Engelen, White, and de Nijs (2003)	The national land cover database of the Netherlands	Generalization	500	17 cell-states	NR	NR	NR	The Netherlands
14	White, Uljee, and Engelen (2012)	CORINE Land Cover data set	Generalization	200, 300	21 cell-states	NR	NR	NR	Greater Dublin Area, Ireland; Belgium
15	Akın, Clarke, and Berberoglu (2014)	Corona, SPOT1, SPOT4, SLOA AVNIR	Object-based classification	10	2: urban, nonurban	NR	NR	NR	Adana, Turkey
16	Herold, Goldstein, and Clarke (2003)	Aerial photos, IKONOS	Visual interpretation	30	2: urban, nonurban	NR	NR	NR	Washington–Baltimore, USA
17	Pijanowski et al. (2009)	Landsat (TM)	Supervised classification	30	4: road, building area, green space and service center	NR	NR	86.1–87.6%	Tehran, Iran
18	Petrov, Lavalle, and Kasanko (2009)	CORINE Land Cover data set	Generalization	100	20 cell-states	NR	NR	NR	Algarve, Portugal
19	Thapa and Murayama (2011)	Corona, Landsat (MSS, TM, ETM+)	ISODATA, ML	30	4: build-up, forest, shrubs, agriculture	Reference data	NR	80.7–84.4%	Kathmandu, Nepal
20	Pontius, Huffaker, and Denman (2004)	MassGIS data set	Generalization	30	2: built, nonbuilt	NR	NR	NR	Ipswich River Watershed, Massachusetts, USA
21	Blanchard, Pontius, and Urban (2015)	MassGIS data set	Generalization	2, 30	2: residential, nonresidential	NR	NR	NR	Lynnfield, Massachusetts, USA
22	Jantz and Goetz (2005)	Landsat (TM, ETM+)	CART algorithm	45, 90, 180, 360	2: urban, nonurban	Reference data	NR	88%	Washington, DC–Baltimore, Maryland, USA

Note: LULC = land-use/land-cover; NR = not rated; ML = maximum likelihood; GCPs = ground control points.

LULC maps generated by the model to the maps generated by random allocation of the changes under the same constraints as employed in the CA model and other naive predicting procedures.

To investigate the relationship between the quality of RS classification and the adequacy of the CA model rules, we analyzed the LULC changes over the 15 × 6 km transect that starts in the center of the city of Netanya, Israel, and extends to surrounding agricultural areas. Our study is based on the outcomes of manual interpretation of high-resolution aerial photos of this area performed over thirty-six years, divided into four intervals of six to eleven years. In parallel, the standard source of the CA modeling—Landsat satellite images of the same area for the same years—is analyzed with several popular pixel-based methods of RS classification and the object-based mean-shift segmentation with the random forest (RF) classification. Based on the output maps, we estimated the LULC changes for each of the employed methods and then the land-use transition probabilities that provide the basis for deriving the CA rules. The LULC changes and transition probabilities estimated from RS imagery were then compared to the LULC changes and land-use transition probabilities estimated from the aerial photos.

We demonstrate that none of the investigated pixel-based methods provided adequate land-use maps that could be exploited for estimating land-use changes and land-use transition probabilities. The mean-shift segmentation with the RF classification algorithms provided close to reality land-use maps but, nonetheless, erroneous estimates of land-use changes and land-use transition matrices.

We thus raise serious doubts regarding the adequacy of CA models of LULC changes, and call the researchers to reexamine the adequacy of data sources and approaches to LULC classification and validation for CA modeling. To encourage this revision of our analysis, we have published the full set of Netanya data at https://drive.google.com/open?id=0B_OK-4hDBIH-Y3hObXV5QkFGaTg.

RS Imagery Classification and Validation for CA Modeling

Typically, CA models consider space as a rectangular grid of square cells that either directly fit to the pixels of the raster data source or aggregate several adjacent cells of the source. Landsat images are the easily available first choice for establishing the CA rules, and in this article we deal with standard Landsat images of 30-m resolution available from the U.S. Geological Survey (USGS) and the Global Land Cover Facility (GLCF) at the University of Maryland. To become an LULC map, an RS image must be classified. Two major classes of the numerous RS imagery classification methods (Lu and Weng 2007) are pixel-based and object-based methods. Pixel-based methods interpret individual pixels, whereas object-based methods aim first at recognizing spatially continuous homogeneous domains of pixels in the image (Yan et al. 2006) and then on interpreting the land uses of these domains.

Table 1 presents details of the data sets and classification methods exploited for establishing the CA rules in twenty-two recent papers on LULC CA modeling. According to these papers, pixel-based classification algorithms are the most common in CA practice, and both unsupervised and supervised classification pixel-based algorithms are exploited.

In this article, we employ the most popular of the pixel-based methods exploited for building CA models of LULC dynamics: two of unsupervised classification (*K*-means and iterative self-organizing data analysis technique [ISODATA]), one of the supervised classification (maximum likelihood [ML]) and one of hybrid classification that combines unsupervised and supervised classification (guided clustering; Bauer et al. 1994).

Object-based classification methods exploit the standard texture and spectral information of an image to recognize continuous homogeneous domains (segments) of the image. Then, supervised classification of these domains is performed. The popularity of LULC object-based classification in change detection RS studies has steadily grown (Yan et al. 2006). These algorithms are still underused in CA studies, however, where the majority of research is still based on simpler, pixel-based methods (Table 1). The accuracy of land-use classification is usually estimated by means of a confusion matrix that measures the fit between the classified map and the LULC map of the "ground truth" for each of the defined LULC classes. The standard aggregate measures of fit between these maps are kappa and overall accuracy statistics (Foody 2002), and recently proposed new measures are quantity and allocation disagreements (Pontius 2000) and fuzzy-kappa (Hagen-Zanker, Straatman, and Uljee 2005). In this article, we limit ourselves to standard measures of fit—overall accuracy (P_c), which estimates the probability of correct classification, and Cohen's kappa (k) index, which estimates the overall error of classification. Typically, the calculations of P_c and k are based on comparison between the classified

LULC map and reference data as a land-use map that serves as the reality or a set of GCPs (Table 1). The probability of correct classification of P_c varies between one and zero, the values of $k = 1$ and $k = -1$ indicate perfect agreement or disagreement between the classified and reference data, and the value of $k = 0$ is expected for the random agreement between the maps. For example, seven out of twenty-two papers listed in Table 1 are based on the classified maps from the National Land Cover (Mitsova, Shuster, and Wang 2011) and CORINE Land Cover (Petrov, Lavalle, and Kasanko 2009; Vaz et al. 2012; White, Uljee, and Engelen 2012) databases. The reported thematic accuracy of the National Land Cover Database is ~80 percent (Wickham et al. 2013) and the CORINE land cover databases claim minimal accuracy of 85 percent (European Environment Agency 2007). The validity of these data is problematic, however, and studies (Feranec et al. 2007; Verbeiren et al. 2013) emphasize that estimates of the total built-up area based on the CORINE database coverage exceed the real value by at least 10 percent.

In what follows, we compare the classified LULC maps obtained with several methods of RS classification, all frequently employed in LULC CA modeling (Table 1), to the reality represented by the maps obtained by the manual classification of aerial photos for the same area. Our goal is to estimate whether the outcome is good enough to serve as a background for LULC CA modeling. We apply various methods of LULC classification to the same set of Landsat images that cover the experimental area and compare the classified maps to the outcome of manual interpretation of aerial photos of that area.

Matrices of Transition Probabilities as a Proxy of the CA Transition Rules

The CA model transition rules depend on the state of a land unit and its neighboring units (Benenson and Torrens 2004), and the essence of the model is the dependence of the transition rules not only on the state of the unit itself but also on the state of its neighbors (Clarke, Hoppen, and Gaydos 1997; White, Engelen, and Uljee 1997; Balzter, Braun, and Köhler 1998; Pontius, Cornell, and Hall 2001; Pijanowski et al. 2002; Soares-Filho, Coutinho Cerqueira, and Lopes Pennachin 2002; Verburg et al. 2002; Paegelow and Olmedo 2005). Given the number k of possible LULC states, an *aggregate* description of the LULC CA state at a current moment t is the row vector $\mathbf{S}(t) = (S_1(t), S_2(t), \ldots, S_k(t))$ representing the numbers $S_i(t)$ of CA cells in states $i = 1, 2, \ldots, k$. The aggregate state $\mathbf{S}(t + 1)$ of the CA at $t + 1$ is, then, defined by the matrix of transition $\mathbf{M}(t, t + 1) = \{p_{ij}\}$ where p_{ij} is a fraction of cells that change their state from i to j. The values of p_{ij} can be considered as probabilities of transition from state i to state j and, in its simplest interpretation, CA can be considered as a Markov process with transition probabilities given by a matrix $\mathbf{M}(t, t + 1)$. In the simplest case, $\mathbf{M}(t, t + 1)$ is constant and does not vary in time; that is, $\mathbf{M}(t, t + 1) = \mathbf{M}$.

Different sets of the CA rules can generate the same transition matrix $\mathbf{M}$. That is, one cannot guarantee that a certain set of rules, despite generating the experimentally estimated transition matrix $\mathbf{M}(t, t + 1)$, will provide an adequate spatial forecast for the LULC map at $t + 1$ based on the LULC pattern at t. The opposite is true: If the transition matrix generated by the CA is different from the one based on the real LULC maps at t and at $t + 1$, then the CA rules are inadequate. That is, the differences between two consecutive LULC maps that serve for estimating the CA rules should adequately represent the changes that happen in reality. The objective of this article is to examine whether the common methods of RS analysis provide sufficiently precise estimates of these changes.

The matrices of LULC transition probabilities provide the basis for estimating CA transition rules. These rules are of numerous types. Some of the CA models, such as DINAMICA EGO (Soares-Filho, Coutinho Cerqueira, and Lopes Pennachin 2002), CA_Markov, and Land Change Modeler modules of the Idrisi GIS (Paegelow and Olmedo 2005) explicitly apply transition probability matrices (TPMs) in each modeled period. In the majority of the CA models, however, including those presented in Table 1, the rules of allocation of the total predicted amount of LULC transitions are more complex.

Our research is based on the LULC dynamics of a part of Netanya city over thirty-six years, registered at five points in time, with intervals varying between six and eleven years. We investigate several classification methods and, employing Landsat images as the standard source of the CA data, we compare TPMs to the matrices based on the reality portrayed in aerial photos.

The next section presents the methodology of the research, followed by the application of the methodology to the data on LULC changes in the city of Netanya over a period of thirty-six years, divided into four intervals. Based on Netanya's case study, we demonstrate the

limitations of the classification methods that are commonly exploited for constructing CA models of LULC dynamics. We then discuss the obtained results.

Method

Study Area

Our area of study is a 15 × 6 km transect that starts in the central business district of the city of Netanya (32°20′0″ N, 34°51′0″ E), crosses it, and extends toward the agricultural and open areas to the east of the city (Figure 1). The transect starts at the seashore and reaches the Samarian hills to the east. Part of the studied area is a unique coastal ecosystem of sand dunes, which is protected by national law. The part beyond the built-up area is a mix of cultivated agriculture, expansion of which is restricted by local and national regulations, and open areas (Orenstein, Frenkel, and Jahshan 2014).

The transect is located in the Sharon district, which is a part of the highly urbanized Tel Aviv metropolitan area. According to the Israeli Central Bureau of Statistics (CBS 2009), nearly 16.6 percent of the area was under residential, public, and industrial construction. In 2008, the population density in the region was 1,122.9 residents/km^2, in comparison with the national average of 323.1 residents/km^2. During the period studied, 1972 to 2008, the population of the city of Netanya and of the entire Sharon district doubled (Table 2).

Construction activities in Netanya and its neighborhood were always high and further accelerated in the early 1990s following a major wave of immigration to Israel. After early 2000, construction declined for several years and then accelerated again (CBS 2009).

Aerial Imagery

The set of aerial imagery that covers the entire transect for the years 1972, 1983, 1993, 1999, and 2008 has been available from the Survey of Israel at a resolution that increases with time (Table 3).

All aerial photos were geometrically rectified and corrected with the ArcGIS 10.3 software (Esri, Redlands, CA, USA) based on the control points that were derived from digital orthophoto images constructed by the Survey of Israel in 2012 at 0.25 m/pixel resolution, georeferenced in the Israeli Transverse Mercator (ITM) coordinate system and combined, for each year, into the full mosaic of the transect. Each mosaic was manually digitized based on natural borders—roads, rivers, forest fringes, and field fringes—and the obtained coverage was classified into the LULC map with six land-use types and thirteen land-cover types (Table 4).

In what follows, we exploit six land uses only and call the vector map resulting from the manual classification of aerial photos the parcel map. For convenient comparison between aerial and satellite imagery-based maps, we rasterize a parcel at 30 × 30 m resolution, following the majority rule. We call the resulting maps the parcel grid.

Landsat Imagery and Classification

The Landsat images of the study area from the USCG and GLCF databases (GLCF, 2013) were available for

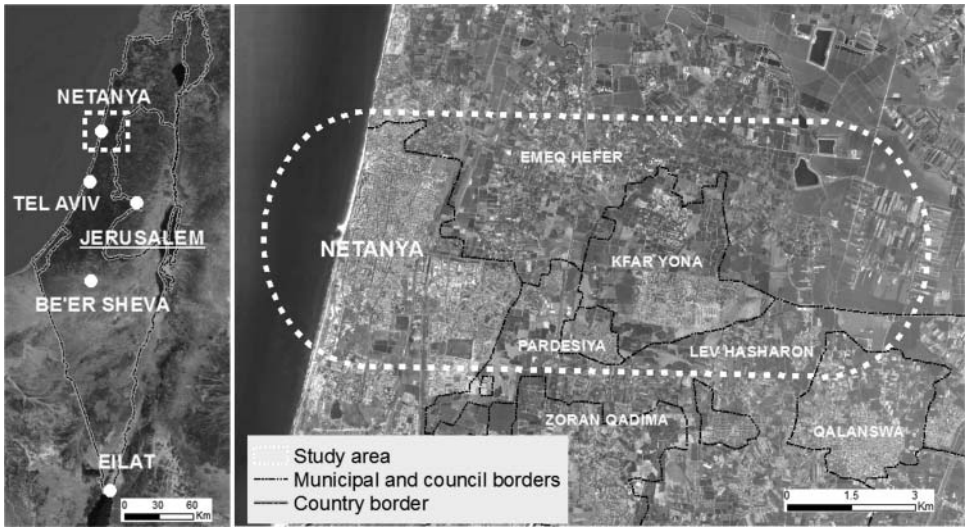

Figure 1. Netanya's transect.

Table 2. Population of Netanya and the Sharon District (CBS 2009)

Population (thousands)	1972	1983	1995	2008
Netanya	71.1	102.3	146.1	180.1
Sharon District	143.5	190.4	275.2	390.8

1972 and 1983, for the same seasons. In three other cases, the Landsat imagery was available for the same season but with one-year shifts between the satellite and the aerial photos: 1992 (instead of 1993), 2000 (instead of 1999), and 2007 (instead of 2008).

All Landsat data were coregistered in the ITM coordinate system and geometrically corrected, preserving 30-m pixel size. To compensate for scene-specific differences in reflectance due to sensor specifications, differences in sun angle, and atmospheric optical thickness, all images were calibrated by histogram matching. The reference for the calibration was the latest Landsat image of 2007. Three bands of the Landsat MSS and four of the TM images were used for classification (Table 5). The cells of the Landsat MSS images of 1972 available at 60-m resolution were resampled (mostly subdivided into four due to a good fit between the cell boundaries) to fit the Landsat TM at 30-m resolution, using a nearest neighbor approach. We interpreted land uses in the Landsat images with four pixel-based and one object-based method.

All exploited pixel-based classification methods are the traditional first choice of a CA modeler:

- *K*-means (unsupervised classification).
- ISODATA (unsupervised classification).
- ML (supervised classification).
- Guided clustering (hybrid classification).

Two unsupervised (*K*-means and ISODATA) classification methods are used most frequently in the CA studies (Table 1). They are both based on pixel spectral characteristics and apply an iterative procedure of clustering that assigns pixels to the cluster with the nearestmean value (Venkateswarlu and Raju 1992; Lu and Weng 2007). The *K*-means method assumes that the number of clusters is known a priori, whereas the ISODATA algorithm follows the logic of the *K*-mean but, additionally, allows merging of clusters or splitting a cluster into two.

Table 3. Resolution of aerial photos, by year

Year	1972	1983	1993	1999	2008
Scale	1:50,000	1:40,000	1:30,000	1:20,000	1:12,000

Table 4. The land use/land cover types identified in the Netanya data set

Land use type	Code	Land cover
Built-up area	BU	BU1: Residential, institutes, public, commercial units in a city
		BU2: Industry, military, cemetery, commercial units outside a city
		BU3: Area under construction
Agriculture	AG	AG1: Cropland, cultivated areas
		AG2: Vineyard, olive and fruit trees, etc.
		AG3: Greenhouse and warehouse
Vegetated area	VG	VG1: Parks, artificial forestation, recreational, sport field, lawns
		VG2: Shrubs, grassland, bare rocks, sparsely vegetated areas
Open space	OS	OS1: Dumps, dunes, beaches, mineral extraction sites
		OS2: Abandoned agricultural and fallow fields
		OS3: Unpaved roads
Water	WA	WA1: Rivers, lakes, reservoirs, sea
Transportation	RD	RD1: Paved roads
		RD2: Rail networks, parking lots

ML is the method of supervised classification that is most popular in CA studies (Benediktsson, Swain, and Ersoy 1989; Paola and Schowengerdt 1995; Ahmad and Quegan 2012). It estimates probabilities of a pixel belonging to one of several predefined LULC classes based on their signatures, and the pixel is then assigned to the class for which the probability is the highest. The ML algorithm is very sensitive to the training signature sampling, and in this article we exploit signatures that are derived from the areas of the Landsat images that correspond to the unambiguous areas representing different LULC classes in the manually classified aerial photos. The hybrid or "guided clustering" merges unsupervised and supervised classification: First, the results of unsupervised ISODATA clustering are exploited as training data to generate spectral signatures of the land uses. Then, based on these signatures, a supervised ML classification is performed (Lillesand and Kiefer 2000). All four pixel-based methods were applied with the ENVI 5.2 software (Canty 2010).

The object-based classification approach involves two steps: segmentation and classification. The method we apply in this article consists of mean-shift

Table 5. Landsat MSS/TM sensor characteristics

Year	Landsat sensor	Resolution (m)	Wavelength (μm) of the spectral channels that were used in classification
1972	MSS	60	Band 1/Green /0.50–0.60
			Band 2/Red/0.60–0.70
			Band 3/Near-infrared/0.70–0.80
1983	TM	30	Band 1/Blue/0.45–0.52
1992			Band 2/Green/0.52–0.60
2000			Band 3/Red/0.63–0.69
2007			Band 4/Near-infrared/0.76–0.90

clustering segmentation (Comaniciu and Meer 2002) and RF classification algorithms (Breiman 2001).

Segmentation of the RS Imagery with Mean-Shift Algorithm

Segmentation aims at partitioning the image into homogeneous segments, based on the similarity of pixel intensities and spatial proximity. Ideally, segments should closely resemble the spatial extent of land-use features presented in the remote sensing image. In this article we apply mean-shift segmentation clustering (Comaniciu and Meer 2002) as implemented in the ENVI/IDL 5.2. software (Canty 2010).

Mean-shift clustering is a mode-seeking segmentation technique that associates each pixel in an image with a spatially aggregated cluster—a segment. Practically, it means that pixels with values that appear most often in a particular region of the image will be aggregated together. The main advantage of the algorithm is that prior information about the number of desired segments is not needed. The algorithm iteratively associates every pixel with locations of the pixels' local maxima, calculated by shifting a search window throughout the image. The windows that end up on the same locations are merged and pixels are clustered into a segment. The detected segment is assigned with the mean value of its pixels.

Random Forest Algorithm of Segment Classification

The RF algorithm is a nonparametric method of supervised image analysis that utilizes classification and regression tree (CART) algorithms (Breiman 2001). The RF algorithm creates an ensemble of random binary trees, where each tree is built for a sample drawn, with replacement, from the reference land-use data set. These trees provide discrete classification predictions, whereas the final decision is made with respect to the class that receives the majority of predictions from all the constructed trees. Tree design maximizes a measure of dissimilarity between land-use classes, measuring the "impurity" of a given segment with respect to the rest of the classes. In this study, the RF algorithm in its CRAN-R implementation (CRAN-R, Version 2.15, R Foundation for Statistical Computing, Vienna, Austria) is applied as the classification step to assign the land uses defined in Table 4 to the segments.

In CRAN-R implementation, the RF classifier demands two parameters for prediction: the desired number of classification trees and the number of prediction variables that are used at each node to make the tree grow.We set the number of trees to 100 and exploited all four available spectral bands of the Landsat imagery as prediction variables.

Transition Probability Matrices

In what follows we characterize the land-use changes by probabilities of transition $p_{ij}(t_0, t_1)$ between uses i and j during time interval (t_0, t_1). Formally, let N be the number of land uses in the area, $S_i(t_0)$ is the total area with use at t_0 of i and the parts of $S_i(t_0)$ that have changed into the uses 1, 2, ..., N during (t_0, t_1) are $S_{i1}(t_1)$, $S_{i2}(t_1)$, ..., $S_{iN}(t_1)$. Then $p_{i1}(t_0, t_1) = S_{i1}(t_1)/S_i(t_0)$, $p_{i2}(t_0, t_1) = S_{i2}(t_1)/S_i(t_0)$, ..., $p_{iN}(t_0, t_1) = S_{iN}(t_1)/S_i(t_0)$.

The state of the land use at t_0 is given by the row vector of the land uses $S(t_0) = (S_1(t_0), S_2(t_0), \ldots, S_N(t_0))$ at t_0 and the land-use dynamics between years t_0 and t_1 are given by matrix $P(t_0, t_1)$ of transition probabilities for the period (t_0, t_1):

$$\mathrm{P}(t_0, t_1) = \begin{pmatrix} p_{11} & p_{12} & \cdots & p_{1N} \\ p_{21} & p_{22} & \cdots & p_{2N} \\ \cdots & \cdots & \cdots & \cdots \\ p_{N1} & p_{N2} & \cdots & p_{NN} \end{pmatrix}, \text{ where } 0 \le p_{ij} < 1 \text{ and } \sum_{j=1}^{N} p_{ij} = 1 \quad (1)$$

In vector form, this can be presented as

$$\mathbf{S(t_1) = S(t_0)^{*}P(t_0, t_1)}.$$

If the probability that a land use i will become j does not depend on the history of a process, then

the land-use changes can be described by the first-order Markov process and the state of the system after several time steps t_1, t_2, …, t_k can be represented as

$$\mathbf{S(t_k) = S(t_0)^* P(t_0,t_1)^* P(t_1,t_2)^* \ldots ^* P(t_{k-1},t_k)}. \quad (2)$$

The values of transition probabilities $p_{ij}(t_0, t_1)$ evidently depend on the length of the time period (t_0, t_1). Typically, for time intervals of several years, the majority of the land uses do not change and the matrix of the land-use transition probabilities for CA has close to unit values on the diagonal. The longer the period of time (t_0, t_1), the lower the diagonal elements $p_{ii}(t_0, t_1)$ and the higher the off-diagonal ones.

Different lengths of the time periods between the years of observation raise the problem of comparing transition matrices obtained for these periods (Takada, Miyamoto, and Hasegawa 2010). Namely, according to Equation 2, if all probabilities are constant but the length of the period (t_1, t_2) is twice as long as the period (t_0, t_1), then $\boldsymbol{P(t_1, t_2) = P(t_0, t_1)^2}$.

To resolve this problem, let us recall that for the simplest case of growth rates r_1 and r_2 given for the periods (t_0, t_1) and (t_1, t_2) time units, respectively, the problem of comparison can be resolved by estimating and comparing growth rates per one time unit: $r_1' = r_1^{(1/(t1 - t0))}$ and $r_2' = r_2^{(1/(t2 - t1))}$. Then, growth rates can be compared for the period of any duration.

A similar procedure can be applied to a positively defined Markov TPM using, in this case, the Jordan normal form (Soares-Filho, Coutinho Cerqueira, and Lopes Pennachin 2002; Flamenco-Sandoval, Martínez Ramos, and Masera 2007); that is, representing $P = P(t_0, t_1)$ as

$$\mathbf{P = AJA^{-1}}, \quad (3)$$

where J is the Jordan normal form of P and A is an invertible matrix. In a common case J is a diagonal matrix with the diagonal elements that are (always positive) eigenvalues of the Markov TPM $\boldsymbol{P = P(t_0, t_1)}$.

In case J is a diagonal matrix, the kth root of a Markov matrix P can be calculated using the kth root of diagonal elements of J:

$$J^{1/k} = \begin{pmatrix} \lambda_1^{1/k} & 0 & \ldots & 0 \\ 0 & \lambda_2^{1/k} & \ldots & 0 \\ \ldots & \ldots & \ldots & \ldots \\ 0 & 0 & \ldots & \lambda_N^{1/k} \end{pmatrix} \quad (4)$$

and, combining Equations 3 and 4:

$$\mathbf{P^{1/k} = AJ^{1/k}A^{-1}}. \quad (5)$$

If Markov matrix P is estimated for the period of k years, then a Markov matrix for the period of m years can be obtained as

$$\mathbf{(P^{1/k})^m = AJ^{m/k}A^{-1}}. \quad (6)$$

Different from the case of the growth rates, the matrix root of the Markov matrix can contain negative elements (Takada, Miyamoto, and Hasegawa 2010) that, evidently, cannot be properly interpreted. We did not encounter this problem in our calculations, however.

Here we normalize Markov matrices for the ten-year period using MATLAB 7.12 software (The MathWorks Inc., Natick, MA, USA). The only modeling software we are aware of that applies a similar approach is DINAMICA EGO, which is mostly oriented to ecological modeling such as urban growth and deforestation (Soares-Filho, Coutinho Cerqueira, and Lopes Pennachin 2002; Maria de Almeida et al. 2003; Thapa and Murayama 2011).

Results

Figure 2 presents parcel grid land-use maps (top left), four maps obtained with the pixel-based methods of satellite image classification, and the map obtained with the segmentation method (top right) for the last available year of the study period, 2007–2008. The rest of the classified images are presented in the Appendix Figure A1.

The segmentation and parcel grid maps are visually similar to each other, whereas the maps of pixel-based classifiers are visually different from them and have an essentially higher percentage of open space areas that are spread over the entire transect. The latter is confirmed by the kappa and accuracy indexes (Foody 2002), calculated with ENVI 5.2 for each of the five classification methods versus the parcel grid map. The values of kappa are the lowest for the clustering ISODATA and

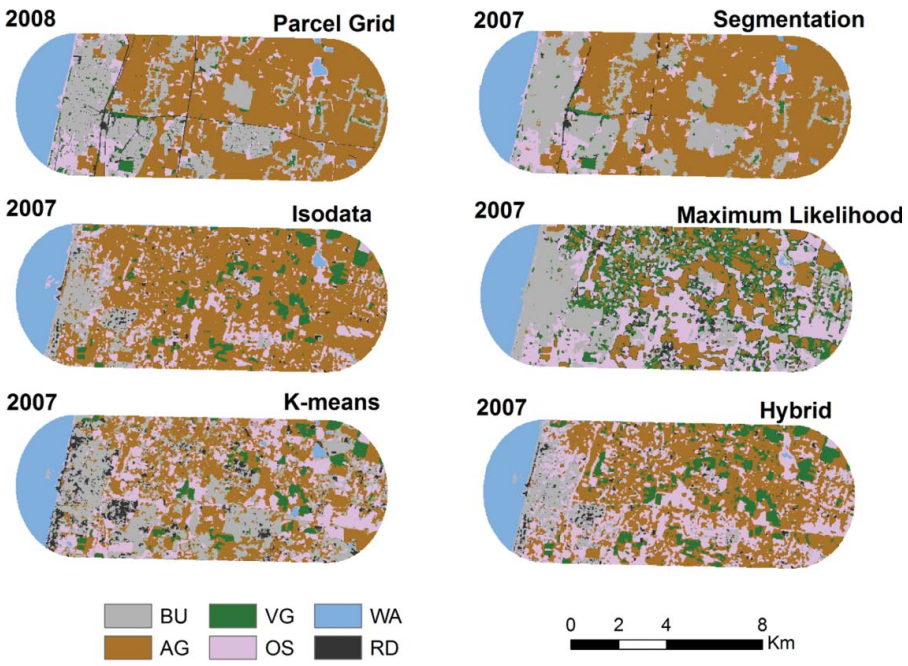

Figure 2. Land-use maps obtained with the manual classification of the aerial photos of 2008 and land-use maps obtained with the help of different classification methods for the Landsat image of 2007. Isodata = iterative self-organizing data analysis technique; BU = built-up; VG = vegetated area; WA = water; AG = agricultural; OS = open space; RD = transportation. (Color figure available online.)

K-means algorithms, intermediate for the hybrid and ML algorithms, and the highest for the segmentation-based classification (Table 6). As can be seen, all four pixel-based classification algorithms performed poorly, whereas the outcome of the segmentation algorithm provides a much better fit to the parcel grid map.

To estimate TPMs, we aggregate six land uses in two ways, into two and three major land-use classes. Two-class aggregation accounts for built-up (BU) and non-built (NB) areas, where the NB area combines all land-use types besides the BU: NB = AG + vegetated area (VG) + open space (OS) + water (WA) + transportation (RD) (Figure 3). Three-class aggregation accounts for built-up (BU), agriculture (AG), and the rest of the areas (RE), where RE = VG + OS + WA + RD.

The preceding aggregation is performed after classification. To assess the effect of a posteriori aggregation, we performed direct classification of the images into urban and nonurban. In this case, the classification was performed after excluding water bodies, as identified in the parcel grid image, from all images.

Note that for the aggregate maps, the values of P_c are much higher, whereas for the three-land-use maps, the values of P_c are close to those obtained for the six-land-use maps, and the kappa index remains at the same level as it is for the six-land-use maps (Table 6). Table 7 presents P_c and kappa index for the two-value and three-value land-use maps. The results of the direct classification of the images with excluded water bodies into two land uses—urban and nonurban—are very close to those obtained for the merged land-use maps (Table 7A) and we do not present them here.

To conclude, the visually low fit between the outcomes of the pixel-based methods and parcel grid is confirmed by the low values of P_c and kappa. That is, the pixel-based maps can hardly serve for estimating TPMs. In what follows, when considering TPMs, we choose the ML classification that performs best among the pixel-based methods and compare among four TPMs that are constructed based on the maps obtained with ML pixel-based, segmentation, parcel grid, and parcel maps methods.

Comparison of Transition Probability Matrices

The full 6 × 6 TPMs estimated for the original time intervals for the segmentation, parcel grid, and parcel-based methods are available online at https://drive.google.com/open?id=0B_OK-4hDBIH-Y3hObXV5QkFGaTg.

The 3 × 3 and 2 × 2 TPM for the aggregated ML, segmentation, parcel grid, and parcel-based maps are also available. In what follows, we illustrate differences based on the ten-year normalized TPM for the aggregate two-land-use and three-land-use maps.

Table 6. P_c and k indexes for the Landsat-based classification versus the parcel grid map

	K-means		ISODATA		Hybrid		ML		Segmentation	
Year	P_C (%)	k	P_C (%)	k	P_C (%)	k	P_C (%)	k	P_C (%)	k
1972	46.5	0.28	44.5	0.28	44.5	0.27	60.4	0.42	87.3	0.78
1983	48.9	0.34	45.4	0.27	47.4	0.32	61.5	0.45	85.5	0.75
1992	40.6	0.22	52.1	0.30	38.4	0.21	48.3	0.35	81.8	0.71
2000	32.0	0.14	48.0	0.29	48.5	0.29	55.1	0.36	79.7	0.68
2007	46.8	0.28	53.4	0.29	45.0	0.24	45.7	0.33	82.4	0.73
Average	43.0	0.25	48.7	0.29	44.8	0.27	54.2	0.38	83.3	0.73

Note: ML = maximum likelihood.

2 × 2 Matrices

Table 8 presents the TPM constructed for the two-value land-use maps. The BU → BU and NB → NB transitions represent areas that did not change during the period. The NB → BU transition describes an urbanization process and is thus the most important for the land-use CA. The BU → NB deurbanization transition could represent urban shrinking. As can be seen in Table 8, the transition probabilities for the various classification methods essentially differ:

No Change Transitions (BU → BU and NB → NB)

The total number of BU → BU transitions for the parcel grid is systematically higher than for the parcel map because roads in the built area usually cover less than 50 percent of the 30 × 30 cell and the built-up cell with roads inside are mostly classified, according to the majority rule, as urban. The effect of the cell size becomes insignificant when the grid resolution is 15 × 15 m (Appendix Figure A2).

The total amount of no change transitions as detected by the segmentation method varies, by periods, more than it does for the parcel grid and parcel map methods. Total amount of no change transitions as detected by the ML method varies greatly and does not reflect the tendencies revealed by three other methods.

The great majority of lands did not change during one time step, providing a high value for P_c. The probability of the BU → BU transition varies between

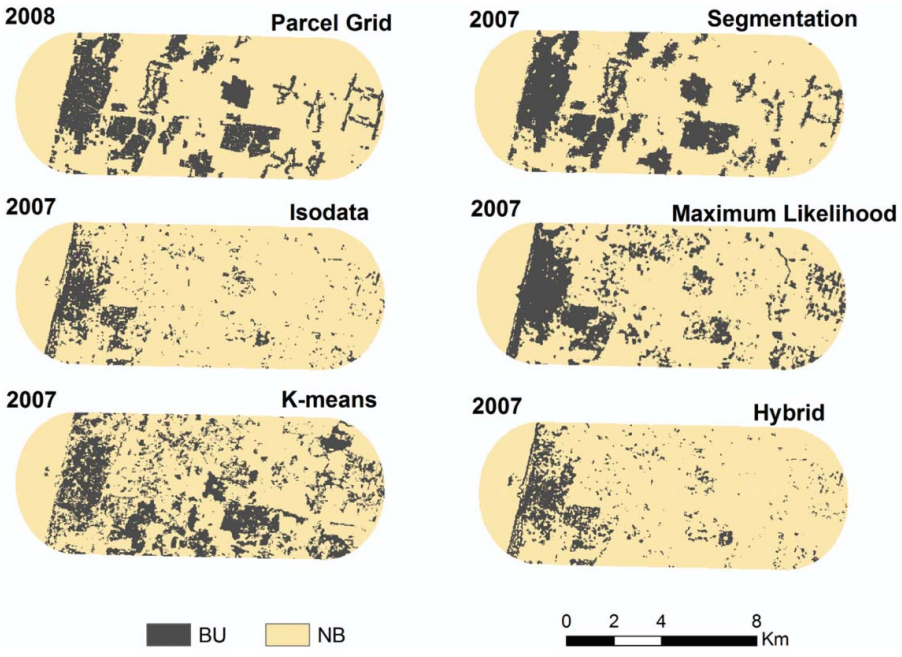

Figure 3. Land-use maps for the built-up and nonbuilt areas, manual classification of the aerial photos of 2008, and various classification methods for the Landsat image of 2007. See Appendix Figure A2 for the maps of the rest of the periods. Isodata = iterative self-organizing data analysis technique; BU = built-up; NB = nonbuilt. (Color figure available online.)

Table 7. P_c and k for the aggregate outputs of the Landsat-based methods versus the parcel grid map for (A) two and (B) three land-use types

(A)

	K-means		ISODATA		Hybrid		ML		Segmentation	
Year	P_C (%)	k	P_C (%)	k	P_C (%)	k	P_C (%)	k	P_C (%)	k
1972	81.9	0.36	83.6	0.45	86.2	0.45	87.2	0.47	92.8	0.72
1983	79.7	0.33	80.4	0.30	85.5	0.40	86.3	0.52	92.2	0.73
1992	80.7	0.37	77.9	0.29	82.9	0.34	86.2	0.52	90.9	0.71
2000	76.9	0.31	74.2	0.32	78.2	0.22	80.9	0.33	88.4	0.68
2007	75.1	0.37	67.9	0.20	78.9	0.35	81.7	0.50	89.8	0.73
Average	78.9	0.35	76.8	0.31	82.3	0.35	84.4	0.47	90.8	0.72

(B)

	K-means		ISODATA		Hybrid		ML		Segmentation	
Year	P_C (%)	k	P_C (%)	k	P_C (%)	k	P_C (%)	k	P_C (%)	k
1972	53.0	0.28	52.1	0.29	68.1	0.46	65.6	0.43	90.1	0.82
1983	53.0	0.31	53.3	0.31	61.2	0.39	64.8	0.45	89.5	0.81
1992	42.9	0.14	42.7	0.15	48.3	0.24	53.7	0.32	86.4	0.77
2000	36.8	0.07	41.8	0.18	44.2	0.20	59.6	0.35	84.5	0.75
2007	50.9	0.27	45.8	0.22	45.6	0.24	50.5	0.30	89.3	0.83
Average	47.3	0.21	47.1	0.23	53.5	0.31	58.8	0.37	88.0	0.80

Note: ML = maximum likelihood.

0.95 and 0.99 for the parcel map and parcel grid and between 0.93 and 0.97 for the NB → NB transitions.

For the segmentation method, the probability of no change for the BU and NB states varies, by periods, between 0.80 and 0.84 and 0.87 and 0.95, respectively, yet is essentially lower than for the parcel map and parcel grid.

For the ML method, the probabilities of no change are essentially lower than for the segmentation method and do not reflect the tendencies revealed by the three other methods.

Probabilities of Transitions Between BU and NB States

According to the Netanya aerial photos, the vast majority of the BU → NB deurbanization transitions are related to the sites that look like construction areas but were abandoned during the period of transition and thus classified as open areas. For the areas classified in a certain year as BU, these changes occur only during the first time interval after this year.

The estimates of the NB → BU transition probabilities for different methods are qualitatively different. NB areas do not have roads. That is why, different from the BU → BU transitions, the total amount of transition from NB → BU is the same for parcel map and parcel grid methods. During the first two periods, the total amount for construction on the NB area is between 2.0 and 2.2 km^2; then it increases twice to 4.7 km^2 for the period of 1993 to 1999 and decreases to 2.5 km^2 again for 2000 to 2007.

For the parcel map and parcel grid, for all periods besides the period of 1972 to 1983, the probability of urbanization NB → BU is much higher than the probability of deurbanization BU → NB. Excluding the period of 1972 to 1983, the average ratio of $p_{NB \to BU}/p_{BU \to NB}$ for the parcel map and parcel grid is close to 4.3. For the 1972 to 1983 period, $p_{NB \to BU}/p_{BU \to NB}$ is 0.75 for the parcel grid and 0.6 for the parcel-based estimates.

Segmentation provides the $p_{NB \to BU}/p_{BU \to NB}$ ratios that are opposite to those obtained with the parcel map and parcel grid methods and vary between 0.31 and 0.68. For the ML the $p_{NB \to BU}/p_{BU \to NB}$ ratios vary even more, between 0.13 and 0.87.

To conclude, for the case of two land-use classes, the TMP matrix obtained with the ML method is qualitatively different from the real TMP matrix in every possible respect. The segmentation method performs much better than pixel-based methods but, despite a relatively good fit between the outcome of the segmentation and parcel-based classifications, the qualitative view of the

Table 8. Transition probability matrices for two-value land-use maps, normalized per ten-year period

		ML			Segmentation			Parcel grid			Parcel map		
		BU	NB	Total	BU	NB	Total	BU	NB	Total	BU	NB	Total
1972–1983 (Landsat and aerial photos)													
p	BU	**0.64**	0.36		**0.84**	0.16		**0.96**	0.04		**0.95**	0.05	
	NB	0.10	**0.90**		0.05	**0.95**		0.03	**0.97**		0.03	**0.97**	
A (km_2)	BU	**7.2**	4.0	11.2	**11.3**	2.1	13.4	**12.3**	0.50	12.8	**11.4**	0.54	11.9
	NB	7.7	**67.3**	75.0	3.7	**69.3**	73.0	2.0	**71.9**	73.9	2.0	**72.6**	74.6
1983–1992 (Landsat)/1983–1993 (aerial photos)													
p	BU	**0.55**	0.45		**0.80**	0.20		**0.99**	0.01		**0.99**	0.01	
	NB	0.06	**0.94**		0.07	**0.93**		0.04	**0.96**		0.03	**0.97**	
A (km_2)	BU	**8.3**	6.8	15.1	**12.4**	2.8	15.2	**14.2**	0.19	14.4	**13.3**	0.13	13.4
	NB	4.6	**66.8**	71.4	4.6	**66.7**	71.3	3.0	**69.2**	72.2	2.2	**71.0**	73.2
1992–2000 (Landsat)/1993–1999 (aerial photos)													
p	BU	**0.37**	0.63		**0.81**	0.19		**0.98**	0.02		**0.98**	0.02	
	NB	0.06	**0.94**		0.13	**0.87**		0.07	**0.93**		0.07	**0.93**	
A (km_2)	BU	**4.9**	8.2	13.1	**13.5**	3.3	16.8	**16.1**	0.35	16.5	**15.1**	0.25	15.4
	NB	4.1	**69.4**	73.5	9.0	**60.7**	69.7	4.7	**65.4**	70.1	4.7	**66.6**	71.3
2000–2007 (Landsat)/1999–2008 (aerial photos)													
p	BU	**0.76**	0.24		**0.77**	0.23		**0.99**	0.01		**0.99**	0.01	
	NB	0.21	**0.79**		0.08	**0.92**		0.05	**0.95**		0.07	**0.93**	
A (km_2)	BU	**7.1**	2.2	9.3	**16.6**	4.9	21.5	**18.9**	0.28	19.2	**17.5**	0.20	17.7
	NB	15.9	**61.2**	77.1	5.2	**59.8**	65.0	3.1	**64.3**	67.4	2.3	**66.6**	68.9

Note: Bold indicates no-change transitions. ML = maximum likelihood; BU = built-up; NB = nonbuilt.

land-use transitions obtained from the Landsat segmentation is opposite to that obtained from the aerial photos.

3 × 3 Matrices

The matrices of transition constructed for three land uses (Table 9) provide additional information on the LULC changes that are related to agriculture lands. Just as in the case of two land uses, the discrepancy between the results of the pixel-based and the rest of the classification methods is very high. We thus exclude pixel-based methods from further discussion and continue with the transition matrices constructed for the segmentation and parcel-based methods only.

Similar to the results obtained for the two land-use classes, the parcel-based estimates of the probability of preserving the same AG and RE land uses are higher than those obtained with the segmentation method. At the same time, larger sizes of agriculture parcels decrease classification error of the segmentation method, and the differences between AG → AG transition probabilities characteristic of segmentation and parcel-based methods are essentially lower than for the BU → BE and RE → RE transitions.

Generally, the probabilities of the AG → BU and RE → BU transitions (i.e., the probability that the nonbuilt area will be built up) are essentially higher for the segmentation than for the parcel-based methods.

As should be expected, the probabilities of transition from the NB to the BU state obtained in two-state classification are unequally split into the AG → BU and RE → BU transitions. The majority of constructions are erected on the RE lands, and the average value of the $p_{RE \to BU}/p_{AG \to BU}$ probabilities ratio for the parcel map and parcel grid methods is 3.3 to 3.5. The segmentation-based estimate of the same ratio is only 2.1.

Estimates of the RE ← → AG transition probabilities based on the segmentation classification are essentially higher than estimates for the parcel grid and parcel map methods. Excluding the 1983 to 1992 or 1983 to 1993 period, $p_{RE \to AG} > p_{AG \to RE}$ for all three classification methods. For the period of 1983 to 1992 or 1983 to 1993, the $p_{RE \to AG} > p_{AG \to RE}$ for the segmentation method, whereas for the parcel-based maps, $p_{RE \to AG} < p_{AG \to RE}$. The average ratio of the $p_{RE \to AG}/p_{AG \to RE}$ for the parcel-based data is 1.6, whereas for the segmentation it is 2.5, essentially higher.

To conclude, segmentation-based transition probabilities between agriculture and the rest of the land uses qualitatively reflect the values obtained by the

Table 9. Ten-year normalized transition probability matrices for three land uses

		ML				Segmentation				Parcel grid				Parcel map			
		BU	AG	RE	Total	BU	AG	RE	Total	BU	AG	RE	Total	BU	AG	RE	Total
1972–1983 (Landsat and aerial photos)																	
p	BU	**0.641**	0.062	0.297		**0.841**	0.110	0.049		**0.963**	0.009	0.028		**0.958**	0.011	0.031	
	AG	0.069	**0.640**	0.291		0.035	**0.919**	0.046		0.018	**0.936**	0.046		0.014	**0.935**	0.051	
	RE	0.139	0.224	**0.637**		0.100	0.131	**0.769**		0.064	0.083	**0.853**		0.051	0.080	**0.869**	
A (km_2)	BU	**7.2**	0.70	3.3	11.2	**11.3**	1.5	0.66	13.5	**12.4**	0.12	0.35	12.9	**11.4**	0.13	0.37	11.9
	AG	2.8	**25.6**	11.6	40.0	1.9	**50.3**	2.5	54.7	0.96	**49.7**	2.4	53.1	0.71	**49.2**	2.7	52.6
	RE	4.9	7.9	**22.5**	35.3	1.8	2.4	**14.1**	18.3	1.3	1.7	**17.5**	20.5	1.1	1.8	**19.1**	22.0
1983–1992 (Landsat)/1983–1993 (aerial photos)																	
p	BU	**0.550**	0.067	0.383		**0.810**	0.132	0.058		**0.987**	0.003	0.010		**0.987**	0.003	0.010	
	AG	0.031	**0.409**	0.560		0.042	**0.904**	0.054		0.015	**0.870**	0.115		0.014	**0.870**	0.116	
	RE	0.096	0.112	**0.792**		0.117	0.155	**0.728**		0.075	0.061	**0.864**		0.064	0.058	**0.878**	
A (km_2)	BU	**8.3**	1.0	5.8	15.1	**12.3**	2.0	0.88	15.2	**14.3**	0.04	0.15	14.5	**13.2**	0.04	0.13	13.4
	AG	1.1	**13.8**	18.9	33.8	2.3	**48.9**	3.0	54.2	0.77	**44.8**	5.9	51.5	0.71	**44.3**	5.9	50.9
	RE	3.6	4.2	**29.8**	37.6	2.0	2.7	**12.5**	17.2	1.5	1.3	**17.8**	20.6	1.4	1.2	**18.9**	21.5
1992–2000 (Landsat)/1993–1999 (aerial photos)																	
p	BU	**0.376**	0.188	0.436		**0.807**	0.133	0.060		**0.984**	0.001	0.015		**0.976**	0.004	0.020	
	AG	0.022	**0.748**	0.230		0.121	**0.796**	0.083		0.051	**0.815**	0.134		0.045	**0.811**	0.144	
	RE	0.063	0.481	**0.456**		0.155	0.201	**0.644**		0.110	0.179	**0.711**		0.091	0.164	**0.745**	
A (km_2)	BU	**4.9**	2.5	5.7	13.1	**13.5**	2.2	1.01	16.7	**16.4**	0.07	0.26	16.7	**14.9**	0.06	0.31	15.3
	AG	0.45	**14.8**	4.6	19.9	6.2	**40.5**	4.2	50.9	2.4	**37.5**	6.2	46.1	2.0	**37.0**	6.6	45.6
	RE	3.4	25.8	**24.4**	53.6	2.9	3.8	**12.1**	18.8	2.6	4.3	**17.0**	23.9	2.3	4.2	**19.1**	25.6
2000–2007 (Landsat)/1999–2008 (aerial photos)																	
p	BU	**0.751**	0.049	0.200		**0.784**	0.131	0.085		**0.993**	0.001	0.006		**0.993**	0.001	0.006	
	AG	0.137	**0.222**	0.641		0.078	**0.859**	0.063		0.020	**0.949**	0.031		0.018	**0.949**	0.033	
	RE	0.325	0.091	**0.584**		0.129	0.126	**0.745**		0.069	0.098	**0.833**		0.054	0.089	**0.857**	
A (km_2)	BU	**7.1**	0.46	1.9	9.5	**16.9**	2.8	1.8	21.5	**19.2**	0.02	0.11	19.3	**17.6**	0.02	0.10	17.7
	AG	5.5	**8.9**	25.9	40.3	3.7	**40.6**	3.0	47.3	0.87	**41.2**	1.3	43.4	0.76	**40.7**	1.4	42.9
	RE	11.9	3.3	**21.4**	36.6	2.3	2.2	**13.2**	17.7	1.7	2.3	**19.9**	23.9	1.4	2.3	**22.3**	26.0

Note: Bold indicates no-change transitions. ML = maximum likelihood; BU = built-up; AG = agricultural; RE = remaining area.

parcel-based classification. Numerically, however, the segmentation-based probability estimates are still different from the parcel-based estimates and will cause essential differences in the model outputs.

Cumulative Versus Directly Estimated Transition Probabilities in the Case of Three Land Uses

The long-term differences between transition matrices can be estimated comparing the probabilities of transition accumulated from the year 1972 to the end of three periods: 1992–1993, 1999–2000, and 2007–2008 (Table 10). In this way, we can estimate whether the sequential application of the TPMs results in the accumulation of error.

The major observations from the cumulative matrix confirm the results based on the TPMs for each period. Directly estimated probabilities of change (off-diagonal elements) are lower than accumulated ones, and the discrepancy increases with time. This discrepancy is lowest for the matrices based on the parcel map, higher for the matrices constructed for the parcel grid maps, and several times higher for the transition probability matrices constructed from the maps classified with the segmentation methods.

Different from the other transition probabilities, directly estimated and accumulated probabilities of the AG → AG (that agriculture land use will not change) are similar for all three methods.

According to the directly estimated transition matrices, for the parcel map and parcel grid maps, the major path of land-use transition is AG → RE → BU. For the segmentation-based maps, AG → BU and AG → RE are equally probable. These tendencies are also seen in accumulated transition matrices, but the absolute values of the probabilities to change land use, according to the accumulated matrices, are 10 to 20 percent higher.

Table 10. Directly estimated versus cumulative transition probability matrices for three land uses (BU, AG, and RE), for three periods, each starting in 1972

		Segmentation			Parcel grid			Parcel map		
		BU	AG	RE	BU	AG	RE	BU	AG	RE
		1972–1992 (Landsat)/1972–1993 (aerial photos)								
p direct	BU	**0.818**	0.139	0.043	**0.959**	0.011	0.030	**0.956**	0.011	0.033
	AG	0.050	**0.851**	0.099	0.029	**0.834**	0.137	0.029	**0.832**	0.139
	RE	0.165	0.132	**0.703**	0.132	0.081	**0.787**	0.110	0.074	**0.816**
p accumulated	BU	**0.692**	0.218	0.090	**0.953**	0.012	0.035	**0.948**	0.014	0.038
	AG	0.072	**0.843**	0.085	0.035	**0.817**	0.148	0.030	**0.817**	0.153
	RE	0.176	0.251	**0.573**	0.129	0.124	**0.747**	0.107	0.120	**0.773**
		1972–2000 (Landsat)/1972–1999 (aerial photos)								
p direct	BU	**0.840**	0.113	0.047	**0.965**	0.007	0.028	**0.961**	0.008	0.031
	AG	0.101	**0.803**	0.096	0.058	**0.791**	0.151	0.055	**0.789**	0.156
	RE	0.255	0.100	**0.645**	0.184	0.062	**0.754**	0.153	0.057	**0.790**
p accumulated	BU	**0.598**	0.284	0.118	**0.942**	0.017	0.041	**0.929**	0.022	0.049
	AG	0.174	**0.697**	0.129	0.093	**0.692**	0.215	0.080	**0.688**	0.232
	RE	0.262	0.338	**0.400**	0.215	0.235	**0.550**	0.180	0.225	**0.595**
		1972–2007 (Landsat)/1972–2008 (aerial photos)								
p direct	BU	**0.892**	0.071	0.037	**0.965**	0.007	0.028	**0.960**	0.007	0.033
	AG	0.109	**0.793**	0.098	0.087	**0.790**	0.123	0.081	**0.788**	0.131
	RE	0.259	0.078	**0.663**	0.215	0.071	**0.714**	0.177	0.066	**0.757**
p accumulated	BU	**0.506**	0.337	0.157	**0.939**	0.021	0.040	**0.926**	0.026	0.048
	AG	0.207	**0.638**	0.155	0.121	**0.678**	0.201	0.105	**0.673**	0.222
	RE	0.283	0.375	**0.342**	0.256	0.277	**0.467**	0.215	0.266	**0.519**

Note: Bold indicates no-change transitions. BU = built-up; AG = agricultural; RE = remaining area.

The largest differences between the directly estimated and accumulated transition probabilities are those of the AG → RE and RE → AG transitions. Accumulated values of these probabilities are essentially higher than directly estimated. This clearly indicates the problem of interpretation of the nonurban land uses.

Discussion and Conclusions

Putting it straightforwardly, our major and novel result is practically a ban on all "easy" parcel-based methods. In our case, these methods cannot even be employed as a source of information for the land-use patterns, because the values of the P_c and kappa indexes are very low. The employed object-based method works much better and provides adequate estimates of the land-use patterns. These patterns are yet imprecise for estimating transition probabilities, however.

Our results basically contradict an essential part of CA practice. With regard to the data sources of the twenty-two papers listed in Table 1, seven employ vector LULC maps acquired from the National Land Cover or CORINE Land Cover databases. Another two are based on the manual interpretation of high-resolution satellite images and aerial photos and are not accompanied by accuracy assessment. The remaining thirteen are based on the direct classification of RS images at resolutions of 30 m or lower from the Landsat TM/ETM+, ASTER, and SPOT satellites. Pixel-based methods are employed in eight papers that report accuracy between 70 percent and 94 percent; four employ object-based methods and report accuracy between 65 percent and 93 percent; and in one of the papers the images were classified manually. That is, at least half of the CA models in Table 1 are based on images that, according to our study, cannot provide correct classification of LULC changes, no matter how high the reported values of P_c and kappa.

At least two reasons for this discrepancy can be proposed:

1. The level of heterogeneity of the area investigated in this article is essentially higher than for the typical area of CA studies. For the exemplar year of 2007–2008, for the 15 × 9 km investigated transect, the average area of an estimated land-use segment is 12.1 ha according to the segmentation and 6.1 ha according to the parcel-based classification (i.e., about 135 and 69 30 × 30 m cells, respectively). Large units of forests,

agriculture, or water area surfaces can essentially increase the values of the P_c and kappa indexes.

2. Selection of the GCPs is not fully random. The GCPs that, unintentionally, are selected beyond the areas of highly mixed land uses can result in higher values of P_c and kappa. Our data make it possible to simulate this nonrandom choice. First, we applied the ArcGIS RegionGroup tool to merge adjacent parcels classified as having identical LULC on a parcel map into larger polygons. Then we constructed a series of buffers of 30-, 60-, 90-, and 120-m width around the boundaries of the obtained polygons. Then, 1,500 GCPs were randomly distributed over the area beyond the buffers. Note that the wider a buffer is, the further away the GCPs are from the boundaries between the continuous areas of the same LULC class. Finally, the values of P_c and kappa for the segmentation- and ML-generated map were estimated.

Nonrandom spread of GCPs "improves" the correctness of the segmentation method (Figure 4): The value of kappa increases from 0.76 to 0.91 when a minimal buffer of 30-m width is considered and reaches 99.0 percent for a buffer width of 120 m. The improvement is less for the ML classification: The accuracy and kappa increase to $P_c = 52.5\%$ and $k = 0.4$ when the buffer width is 60 m and to 57.5 percent and 0.45 percent when the buffer width is 120 m.

This and other possible explanations do not simplify the problem. The focus of CA study is, undoubtedly, on the borders between homogeneous areas. These are

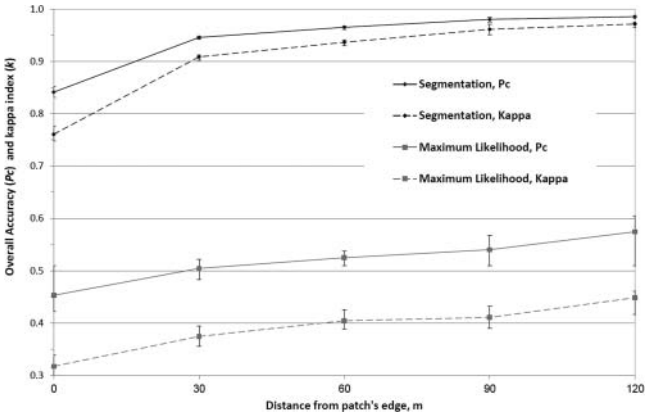

Figure 4. Overall accuracy P_c and kappa as dependent on the width of buffer around the parcels' boundaries based on the Landsat 2007 image. For the entire image, $P_c = 84.2\%$ and $\kappa = 0.73$ for the segmentation method, and $P_c = 45.7\%$ and $\kappa = 0.33$ for the maximum likelihood method.

the lands where the majority of land-use changes take place. These boundaries, themselves, move in space. Pixel-based classification methods have inherent problems when classifying pixels with reflectance that is defined by two or more land-cover types and, as we have demonstrated in this article, the segmentation method cannot fully avoid these problems either. That is, even the standard level of accuracy characterized by P_c (~80–85 percent) and k (~0.75–0.8) does not guarantee a correct estimate of the transition probabilities. Generally, although high overall accuracy of classification is necessary for CA modeling of the LULC dynamics, it is still insufficient. Local classification errors can propagate and, in case important but local changes are missed, the CA model dynamics can still significantly deviate from the reality. These issues go far beyond the topic of our article and are discussed in depth in Chapter 9 of White, Engelen, and Uljee (2015).

Uncertainties in RS data for simulation LULC dynamics have been raised by several authors (Pontius, Huffaker, and Denman 2004; van der Kwast et al. 2009; Pontius and Petrova 2010). Among them, Pontius and Petrova (2010) proposed the most comprehensive model assessment and validation procedure, which is based on a series of comparisons between reference maps representing the built and nonbuilt area at several time moments and the maps generated for the same time moments by the CA model. Any method of assessment and validation demands reference LULC maps that properly reflect real-world land uses and covers. As we demonstrate, the initial data for constructing these maps and the classification methods should be chosen with great care.

Our article clearly raises demand for a critical revision of the entire CA framework. We claim that the current "optimistic" view, which takes for granted that the modeler possesses adequate estimates of land-use patterns and land-use changes, should be substituted by the positivistic CA framework that builds on carefully validated and commonly available depositories of land-use maps.

Here were initiate the list of constraints that should be imposed on CA-oriented classification:

- Vector-based CA that inherently account for parcels' boundaries should be preferred over cell-based CA.
- The resolution of satellite images used in CA studies should be high, 10 m and below. Landsat images of

lower resolution cannot be the only source of information.
- All estimates of changes should be normalized regarding the same time unit.
- Land-use classification should be carefully validated. Validation should be focused on the boundaries between the land uses. GCPs located within the internal parts of large homogeneous forests or agriculture areas are of low value for CA-oriented classification.

We appeal for a new perspective on CA modeling: In the future, it should be based on a series of a high-resolution, carefully validated, long-term land-use maps that reflect different types of land-use dynamics and represent different types of land planning systems and different periods of population growth and economic development. The accompanying metadata on historical events and trends will have major value for proper model calibration and validation.

Acknowledgments

We are grateful to two anonymous reviewers for helpful comments on earlier drafts of the article. Many thanks to Carole Shoval for language assistance and editing.

There is always a chance that we are wrong in our choice of method's parameters, RS software, or interpretation of results. Understanding the importance of our results for the future of CA modeling, we make our data and results available at https://drive.google.com/open?id=0B_OK-4hDBIH-Y3hObXV5QkFGaTg. The site contains initial data sets, full transition matrices for six land-use types, and other supplementary materials. The reader is cordially invited to employ all possible classification methods and to upload their classification results for comparison.

References

Ahmad, A., and S. Quegan. 2012. Analysis of maximum likelihood classification technique on Landsat 5 TM satellite data of tropical land covers. Paper presented at Control System, Computing and Engineering (ICCSCE), 2012 IEEE International Conference, Penang, Malaysia.

Akın, A., K. C. Clarke, and S. Berberoglu. 2014. The impact of historical exclusion on the calibration of the SLEUTH urban growth model. *International Journal of Applied Earth Observation and Geoinformation* 27 (Part B): 156–68.

Araya, Y. H., and P. Cabral. 2010. Analysis and modeling of urban land cover change in Setúbal and Sesimbra, Portugal. *Remote Sensing* 2 (6): 1549–63.

Arsanjani, J. J., W. Kainz, and A. J. Mousivand. 2011. Tracking dynamic land-use change using spatially explicit Markov chain based on cellular automata: The case of Tehran. *International Journal of Image and Data Fusion* 2 (4): 329–45.

Balmann, A. 1997. Farm-based modelling of regional structural change: A cellular automata approach. *European Review of Agricultural Economics* 24 (1): 85–108.

Balzter, H., P. W. Braun, and W. Köhler. 1998. Cellular automata models for vegetation dynamics. *Ecological Modelling* 107 (2–3): 113–25.

Batty, M., Y. Xie, and Z. Sun. 1999. Modeling urban dynamics through GIS-based cellular automata. *Computers, Environment and Urban Systems* 23:205–33.

Bauer, M. E., T. E. Burk, A. R. Ek, P. R. Coppin, S. D. Lime, D. K. Walters, T. A. Walsh, W. Befort, and D. F. Heinzen. 1994. Satellite inventory of Minnesota forests. *Photogrammetric Engineering and Remote Sensing* 60 (3): 287–98.

Benediktsson, J. A., P. H. Swain, and O. K. Ersoy. 1989. Neural network approaches versus statistical methods in classification of multisource remote sensing data. Paper presented at the Geoscience and Remote Sensing Symposium, 12th Canadian Symposium on Remote Sensing, Vancouver, Canada.

Benenson, I., and P. M. Torrens. 2004. *Geosimulation: Automata-based modeling of urban phenomena*. New York: Wiley

Blanchard, S. D., R. G. Pontius, Jr., and K. M. Urban. 2015. Implications of using 2 m versus 30 m spatial resolution data for suburban residential land change odeling. *Journal of Environmental Informatics* 25 (1): 1–13.

Breiman, L. 2001. Random forests. *Machine Learning* 45 (1): 5–32.

Candau, J. C., and K. C. Clarke. 2000. Probabilistic land cover modeling using deltatrons. Paper presented at the 38th annual conference of the Urban Regional Information Systems Association. Orlando, FL.

Canty, M. J. 2010. *Image analysis, classification, and change detection in remote sensing: With algorithms for ENVI/IDL*. 2nd ed. Boca Raton, FL: CRC.

Central Bureau of Statistics (CBS). 2009. *Statistical abstract of Israel (60). Ministry of Interior*. http://www.cbs.gov.il/ (last accessed 19 May 2015).

Chen, Q., and A. E. Mynett. 2003. Effects of cell size and configuration in cellular automata based prey–predator modelling. *Simulation Modelling Practice and Theory* 11 (7–8): 609–25.

Clarke, K. C., S. Hoppen, and L. Gaydos. 1996. A self-modifying cellular automata model of historical urbanization in the San Francisco Bay area. *Environment and Planning B: Planning and Design* 24:247–61.

Clarke, K. C., S. Hoppen, and L. J. Gaydos. 1997. A self-modifying cellular automaton model of historical urbanization in the San Francisco Bay area. *Environment and Planning B: Planning and Design* 24:247–61.

Comaniciu, D., and P. Meer. 2002. Mean shift: A robust approach toward feature space analysis. *IEEE Transactions on Pattern Analysis and Machine Intelligence* 24 (5): 603–19.

Dietzel, C., and K. Clarke. 2006. The effect of disaggregating land use categories in cellular automata during model calibration and forecasting. *Computers, Environment and Urban Systems* 30 (1): 78–101.

Dietzel, C., and K. C. Clarke. 2007. Toward optimal calibration of the SLEUTH land use change model. *Transactions in GIS* 11 (1): 29–45.

Du, Y., W. Wen, F. Cao, and M. Ji. 2010. A case-based reasoning approach for land use change prediction. *Expert Systems with Applications* 37 (8): 5745–50.

European Environmental Agency (EEA). 2007. Technical report. Vol 17. CLC2006 technical guidelines. Copenhagen, Denmark.

Engelen, G., R. White, and T. de Nijs. 2003. Environment explorer: Spatial support system for the integrated assessment of socio-economic and environmental policies in The Netherlands. *Integrated Assessment* 4 (2): 97–105.

Fan, F., Y. Wang, and Z. Wang. 2008. Temporal and spatial change detecting (1998–2003) and predicting of land use and land cover in core corridor of Pearl River Delta (China) by using TM and ETM+ images. *Environmental Monitoring and Assessment* 137 (1–3): 127–47.

Feranec, J., G. Hazeu, S. Christensen, and G. Jaffrain. 2007. CORINE land cover change detection in Europe (case studies of The Netherlands and Slovakia). *Land Use Policy* 24 (1): 234–47.

Flamenco-Sandoval, A., M. Martínez Ramos, and O. R. Masera. 2007. Assessing implications of land-use and land-cover change dynamics for conservation of a highly diverse tropical rain forest. *Biological Conservation* 138 (1–2): 131–45.

Foody, G. M. 2002. Status of land cover classification accuracy assessment. *Remote Sensing of Environment* 80 (1): 185–201.

Global Land Cover Facility (GLCF). 2013. *Global Land Cover Facility*. USGS. www.landcover.org (last accessed 23 June 2013).

Guan, D., H. Li, T. Inohae, W. Su, T. Nagaie, and K. Hokao. 2011. Modeling urban land use change by the integration of cellular automaton and Markov model. *Ecological Modelling* 222 (20–22): 3761–72.

Hagen-Zanker, A., B. Straatman, and I. Uljee. 2005. Further developments of a fuzzy set map comparison approach. *International Journal of Geographical Information Science* 19 (7): 769–85.

Hagen-Zanker, A., J. van Loon, A. Maas, B. Straatman, T. de Nijs, and G. Engelen. 2005. Measuring performance of land use models: An evaluation framework for the calibration and validation of integrated land use models featuring cellular automata. Paper presented at the 14th European Colloquium on Quantitative Geography, Tomar, Portugal.

Hall, F. G., D. B. Botkin, D. E. Strebel, K. D. Woods, and S. J. Goetz. 1991. Large-scale patterns of forest succession as determined by remote sensing. *Ecology* 72 (2): 628–40.

Herold, M., N. C. Goldstein, and K. C. Clarke. 2003. The spatiotemporal form of urban growth: Measurement, analysis and modeling. *Remote Sensing of Environment* 86 (3): 286–302.

Jantz, C. A., and S. J. Goetz. 2005. Analysis of scale dependencies in an urban land-use-change model. *International Journal of Geographical Information Science* 9 (2): 217–41.

Kamusoko, C., M. Aniya, B. Adi, and M. Manjoro. 2009. Rural sustainability under threat in Zimbabwe—Simulation of future land use/cover changes in the Bindura district based on the Markov-cellular automata model. *Applied Geography* 29 (3): 435–47.

Li, X., and A. G. O. Yeh. 2001. Calibration of cellular automata by using neural networks for the simulation of complex urban systems. *Environment and Planning A* 33 (8): 1445–62.

Lillesand, T. M., and R. W. Kiefer. 2000. *Remote sensing and image interpratation*. 4th ed. New York: Wiley.

Liu, X., and C. Andersson. 2004. Assessing the impact of temporal dynamics on land-use change modeling. *Computers, Environment and Urban Systems* 28 (1–2): 107–24.

Logofet, D. O., and V. N. Korotkov. 2002. "Hybrid" optimisation: A heuristic solution to the Markov-chain calibration problem. *Ecological Modelling* 151 (1): 51–61.

Lu, D., and Q. Weng. 2007. A survey of image classification methods and techniques for improving classification performance. *International Journal of Remote Sensing* 28 (5): 823–70.

Maria de Almeida, C., M. Batty, A. M. Vieira Monteiro, G. Câmara, B. S. Soares-Filho, G. C. Cerqueira, and C. L. Pennachin. 2003. Stochastic cellular automata modeling of urban land use dynamics: Empirical development and estimation. *Computers, Environment and Urban Systems* 27 (5): 481–509.

Mitsova, D., W. Shuster, and X. Wang. 2011. A cellular automata model of land cover change to integrate urban growth with open space conservation. *Landscape and Urban Planning* 99 (2): 141–53.

Mondal, P., and J. Southworth. 2010. Evaluation of conservation interventions using a cellular automata–Markov model. *Forest Ecology and Management* 260 (10): 1716–25.

Myint, S. W., and L. Wang. 2006. Multicriteria decision approach for land use land cover change using Markov chain analysis and a cellular automata approach. *Canadian Journal of Remote Sensing* 32 (6): 390–404.

Norman, L. M., M. Feller, and M. L. Villarreal. 2012. Developing spatially explicit footprints of plausible land-use scenarios in the Santa Cruz Watershed, Arizona and Sonora. *Landscape and Urban Planning* 107 (3): 225–35.

Orenstein, D. E., A. Frenkel, and F. Jahshan. 2014. Methodology matters: Measuring urban spatial development using alternative methods. *Environment and Planning B: Planning and Design* 41 (1): 3–23.

Paegelow, M., and M. T. C. Olmedo. 2005. Possibilities and limits of prospective GIS land cover modelling—A compared case study: Garrotxes (France) and Alta Alpujarra Granadina (Spain). *International Journal of Geographical Information Science* 19 (6): 697–722.

Paola, J. D., and R. A. Schowengerdt. 1995. A detailed comparison of backpropagation neural network and maximum-likelihood classifiers for urban land use

classification. *IEEE Transactions on Geoscience and Remote Sensing* 33 (4): 981–96.
Petrov, L. O., C. Lavalle, and M. Kasanko. 2009. Urban land use scenarios for a tourist region in Europe: Applying the MOLAND model to Algarve, Portugal. *Landscape and Urban Planning* 92 (1): 10–23.
Pijanowski, B. C., D. G. Brown, B. A. Shellito, and G. A. Manik. 2002. Using neural networks and GIS to forecast land use changes: A land transformation model. *Computers, Environment and Urban Systems* 26 (6): 553–75.
Pijanowski, B. C., S. Pithadia, B. A. Shellito, and K. Alexadridis. 2005. Calibrating a neural network-based urban change model for two metropolitan areas of the Upper Midwest of the United States. *International Journal of Geographical Information Science* 19 (2): 197–215.
Pijanowski, B. C., A. Tayyebi, M. R. Delavar, and M. J. Yazdanpanah. 2009. Urban expansion simulation using geospatial information system and artificial neural networks. *International Journal of Environmental Research* 3 (4): 493–502.
Pontius, R. G., Jr. 2000. Quantification error versus location error in comparison of categorical maps. *Photogrammetric Engineering and Remote Sensing* 66 (8): 1011–16.
———. 2002. Statistical methods to partition effects of quantity and location during comparison of categorical maps at multiple resolution. *Photogrammetric Engineering & Remote Sensing* 68 (10): 1041–49.
Pontius, R. G., Jr., J. D. Cornell, and C. A. S. Hall. 2001. Modeling the spatial pattern of land-use changes with GEOMOD2: Application and validation for Costa Rica. *Agriculture, Ecosystems and Environment* 1175: 1–13.
Pontius, R. G., Jr., D. Huffaker, and K. Denman. 2004. Useful techniques of validation for spatially explicit land-change models. *Ecological Modelling* 179 (4): 445–61.
Pontius, R., Jr., and N. Malizia. 2004. Effect of category aggregation on map comparison. In *Geographic information science*, ed. M. Egenhofer, C. Freksa, and H. Miller, 251–68. Berlin: Springer.
Pontius, R. G., Jr., and S. H. Petrova. 2010. Assessing a predictive model of land change using uncertain data. *Environmental Modelling & Software* 25 (3): 299–309.
Puertas, O. L., C. Henríquez, and F. J. Meza. 2014. Assessing spatial dynamics of urban growth using an integrated land use model: Application in Santiago Metropolitan area, 2010–2045. *Land Use Policy* 38:415–25.
Shafizadeh Moghadam, H., and M. Helbich. 2013. Spatiotemporal urbanization processes in the megacity of Mumbai, India: A Markov chains-cellular automata urban growth model. *Applied Geography* 40:140–49.
Silva, E. A., and K. C. Clarke. 2002. Calibration of the SLEUTH urban growth model for Lisbon and Porto, Portugal. *Computers, Environment and Urban Systems* 26 (6): 525–52.
Soares-Filho, B. S., G. Coutinho Cerqueira, and C. Lopes Pennachin. 2002. Dinamica—A stochastic cellular automata model designed to simulate the landscape dynamics in an Amazonian colonization frontier. *Ecological Modelling* 154 (3): 217–35.
Stevens, D., S. Dragicevic, and K. Rothley. 2007. iCity: A GIS–CA modelling tool for urban planning and decision making. *Environmental Modelling & Software* 22 (6): 761–73.
Straatman, B., R. White, and G. Engelen. 2004. Towards an automatic calibration procedure for constrained cellular automata. *Computers, Environment and Urban Systems* 28 (1–2): 149–70.
Takada, T., A. Miyamoto, and S. Hasegawa. 2010. Derivation of a yearly transition probability matrix for land-use dynamics and its applications. *Landscape Ecology* 25 (4): 561–72.
Thapa, R. B., and Y. Murayama. 2011. Urban growth modeling of Kathmandu metropolitan region, Nepal. *Computers, Environment and Urban Systems* 35 (1): 25–34.
Torrens, P. M. 2011. Calibrating and validating cellular automata models of urbanization. In *Urban remote sensing: Monitoring, synthesis and modeling in the urban environment*, ed X. Yang, 335–45. Chichester, UK: Wiley.
van der Kwast, J., I. Uljee, G. Enegelen, T. Van de Voorde, F. Canters, and C. Lavalle. 2009. Using remote sensing derived spatial metrics for the calibration of land-use change models. Paper presented at 7th International Urban Remote Sensing Conference, Shanghai, China.
Vaz, E. D. N., P. Nijkamp, M. Painho, and M. Caetano. 2012. A multi-scenario forecast of urban change: A study on urban growth in the Algarve. *Landscape and Urban Planning* 104 (2): 201–11.
Venkateswarlu, N. B., and P. S. V. S. K. Raju. 1992. Fast isodata clustering algorithms. *Pattern Recognition* 25 (3): 335–42.
Verbeiren, B., T. Van De Voorde, F. Canters, M. Binard, Y. Cornet, and O. Batelaan. 2013. Assessing urbanisation effects on rainfall-runoff using a remote sensing supported modelling strategy. *International Journal of Applied Earth Observation and Geoinformation* 21:92–102.
Verburg, P. H., W. Soepboer, A. Veldkamp, R. Limpiada, and V. Espaldon. 2002. Modeling the spatial dynamics of regional land use: The CLUE-S model. *Environmental Management* 30 (3): 391–405.
Wang, S. Q., X. Q. Zheng, and X. B. Zang. 2012. Accuracy assessments of land use change simulation based on Markov-cellular automata model. *Procedia Environmental Sciences* 13:1238–45.
White, R., and G. Engelen. 1993. Cellular-automata and fractal urban form—A cellular modeling approach to the evolution of urban land-use patterns. *Environment and Planning A* 25 (8): 1175–99.
White, R., G. Engelen, and I. Uljee. 1997. The use of constrained cellular automata for high-resolution modelling of urban land-use dynamics. *Environment and Planning B: Planning and Design* 24 (3): 323–43.
———. 2015. *Modeling cities and regions as complex systems: From theory to planning applications*. Cambridge, MA: MIT Press.
White, R., I. Uljee, and G. Engelen. 2012. Integrated modelling of population, employment and land-use change with a multiple activity-based variable grid cellular automaton. *International Journal of Geographical Information Science* 26 (7): 1251–80.
Wickham, J. D., S. V. Stehman, L. Gass, J. Dewitz, J. A. Fry, and T. G. Wade. 2013. Accuracy assessment of NLCD 2006 land cover and impervious surface. *Remote Sensing of Environment* 130:294–304.

Wu, F. 1998. Simulating urban encroachment on rural land with fuzzy-logic-controlled cellular automata in a geographical information system. *Journal of Environmental Management* 53 (4): 293–308.

———. 2002. Calibration of stochastic cellular automata: The application to rural–urban land conversions. *International Journal of Geographical Information Science* 16 (8): 795–818.

Wu, F., and C. J. Webster. 1998. Simulation of land development through the integration of cellular automata and multicriteria evaluation. *Environment and Planning B: Planning and Design* 25 (1): 103–26.

Xi, F., H. S. He, Y. Hu, R. Bu, Y. Chang, X. Wu, M. Liu, and T. Shi. 2010. Simulating the impacts of ecological protection policies on urban land use sustainability in Shenyang-Fushun, China. *International Journal of Urban Sustainable Development* 1 (1–2): 111–27.

Yan, G., J. F. Mas, B. H. P. Maathuis, Z. Xiangmin, and P. M. Van Dijk. 2006. Comparison of pixel-based and object-oriented image classification approaches—A case study in a coal fire area, Wuda, Inner Mongolia, China. *International Journal of Remote Sensing* 27 (18): 4039–55.

YULIA GRINBLAT is a PhD candidate at the Porter School of Environmental Studies and a member of Geosimulation and Spatial Analysis Laboratory at the Department of Geography and Human Environment, Tel Aviv University, Tel Aviv 69978, Israel. E-mail: juliagri@post.tau.ac.il. Her main interests include spatial–temporal analysis and modeling of land-use changes along fringe landscapes.

MICHAEL GILICHINSKY is a remote sensing specialist and at the time of the presented research he was a research fellow at the Samaria and Jordan Rift R&D Center, Ariel University, Ariel 40700, Israel. E-mail: gilichinsky@gmail.com. His research interests include the applications of optical remote sensing methods for land use and land cover mapping.

ITZHAK BENENSON is Professor of Geography and head of the Geosimulation and Spatial Analysis lab in the Department of Geography and Human Environment, Tel Aviv University, Tel Aviv 69978, Israel. E-mail: bennya@post.tau.ac.il. His research includes study of big urban data, modeling of urban land use and residential dynamics, impact of local and regional plans, use of public transport and parking in the city, vehicle–pedestrian interactions, and road accidents.

Appendix

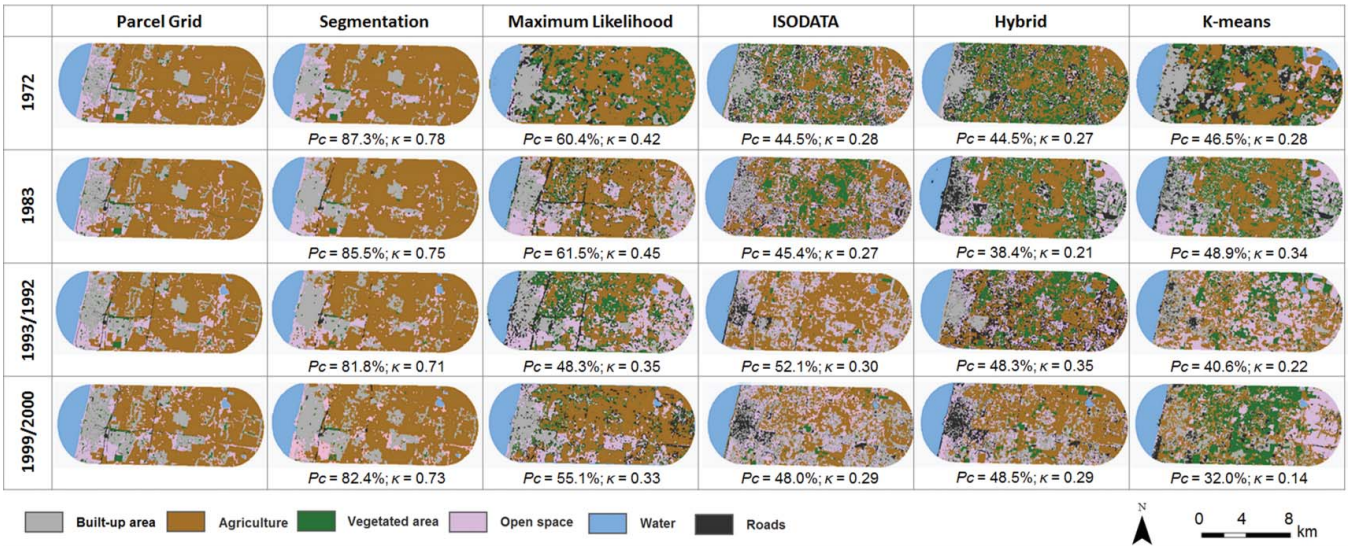

Figure A1. Land-use maps obtained with the manual classification of the aerial photos and land-use maps obtained with the help of various classification methods for the Landsat images. The columns are ordered according to the average value, by years, of the accuracy P_c. ISODATA = iterative self-organizing data analysis technique. (Color figure available online.)

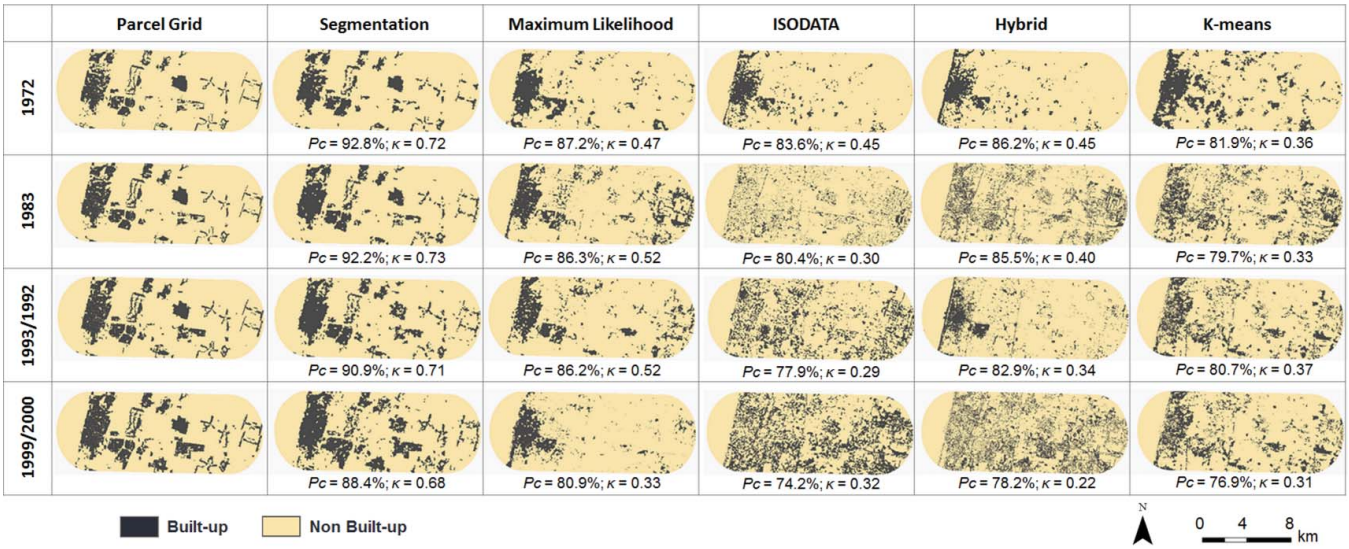

Figure A2. Land-use maps for built-up and nonbuilt areas, compiled by manual classification of aerial photos and various classification methods for the Landsat images. The columns are ordered as in the figure of the Appendix. ISODATA = iterative self-organizing data analysis technique. (Color figure available online.)